Materials Research. 2021; 24(2): e20200485
DOI: https://doi.org/10.1590/1980-5373-MR-2020-0485

Refractory Ceramics of Clay and Alumina Waste

Valmir José da Silva[a], Salvador K. A. Taveira[a], Karina R. Silva[a], Gelmires A. Neves[a], Hélio L. Lira[a], Lisiane N. L. Santana[a]*

[a]*Universidade Federal de Campina Grande – UFCG, Unidade Acadêmica de Engenharia de Materiais, Av. Aprígio Veloso, 882, Cep 58109-970, Bodocongó, Campina Grande, PB, Brasil*

Received: October 21, 2020; Revised: November 23, 2020; Accepted: December 28, 2020

Refractory ceramics were produced from clays and alumina waste. Specimens were shaped by uniaxial pressing, subjected to thermal analysis by dilatometry and heat-treated in a conventional furnace at 1300 and 1400ºC, applying a heating rate of 5ºC/min and a dwell time of 2 and 3 hours at the maximum temperature. The samples were characterized by X-ray diffraction (XRD), scanning electron microscopy (SEM) and physicomechanical properties. The dilatometric analysis before heat treatment indicated that the formulation containing the largest amount of fluxing oxides presented the highest linear shrinkage. The XRD analysis revealed that mullite was the major phase and needle shaped crystals typical of mullite obtained from clay minerals were observed by SEM. The increase in firing temperature and dwell time at the maximum temperature improved the physicomechanical properties of the specimens. The thermal expansion coefficient (TEC) in the range of 25 to 1000ºC varied from 6.2 to 6.9 x 10^{-6}ºC^{-1}.

Keywords: *Clays, alumina waste, refractory ceramics.*

1. Introduction

Refractory ceramics are materials that do not undergo any physical or chemical change when used in high temperature applications. The main thermomechanical and thermophysical properties of refractories are related to their ability to withstand different degrees of thermal and mechanical stresses, and to resist corrosion by liquids and gases[1,2]. These properties depend on the characteristics of raw materials and formulations (chemical and mineralogical composition, particle size and shape distribution) the forming process and sintering temperature[3-5].

Different types of refractories can be produced depending on the kind of raw materials and the processing parameters[3]. Compositions containing silica and alumina are extensively studied. After heat treatment, these compositions generate mullite and corundum (α-Al_2O_3), which applications include furnace linings, refractory supports and thermal insulation[2].

Mullite is one of the most important refractory ceramics, because of its unique combination of properties: high melting point (~ 1800ºC), excellent mechanical and thermal shock resistance, chemical stability, low thermal expansion coefficient, low thermal conductivity at high temperatures, low dielectric constant, and its ability to act as an electrical insulator, making it potentially useful in various applications from refractories to electronic substrates[3,6-13].

An alternative to synthesize mullite refractories at a lower cost is to use natural raw materials such as clay minerals, which have considerable amounts of aluminum (Al_2O_3) and silicon (SiO_2) oxides. However, due to the low Al_2O_3/SiO_2 ratio of these materials, alumina precursors should be added to balance this ratio, thereby formulating stoichiometrically suitable compositions to obtain mullite as the major phase. The alumina production process (the Bayer process) generates a waste with a high content of Al_2O_3, which has been studied as a possible precursor for this purpose.

Concern about environmental issues around the world has grown in recent decades, especially in the academic community and research has strongly focused on the development of sustainable methods aimed at recycling inorganic waste[14-24]. Many studies have emphasized interest in the development of compositions suitable for the production of refractories coatings used in ovens.

The aim of this research was to prepare ceramic refractories from industrial alumina waste and clays. The effects of alumina waste content and sintering parameters (dwell time and temperature) on phase composition, microstructural, mechanical, physical and thermal properties were analysed. The effective use of waste materials not only helps to solve a complex environmental problem such as pollution and the conservation of natural resources, but also produces materials with high added value.

2. Experimental Procedures

Two clays (X and Y) and alumina waste (AW) were used as precursor raw materials for the production of test specimens. The clays were subjected to a chemical analysis using a Shimadzu EDX-720 energy dispersive X-ray fluorescence spectrometer. The alumina waste had an Al_2O_3 content of > 90%. The mineralogical, granulometric and thermal characterization of AW was described by Silva et al.[25]

*e-mail: helio.lira@ufcg.edu.br

After analyzing the chemical composition of the precursors, two formulations were prepared, using the stoichiometric form of mullite ($3Al_2O_3.2SiO_2$), which were called S1 (57.7 wt.% of clay X + 42.3 wt.% of AW) and S2 (53.3 wt.% of clay Y + 46.7 wt.% of AW). The formulations were subjected to chemical characterization (Table 1) by X-ray fluorescence, using a Shimadzu EDX-720 energy dispersive X-ray fluorescence spectrometer and mineralogical characterization by X-ray diffraction using a Shimadzu XRD-6000 X-ray diffractometer operating with CuKα radiation, 40 kV voltage, 30 mA current, step size of 0.02° and 2θ sweep angle varying from 5 to 60º.

The particle size of the formulations was analyzed using a CILAS 1090 particle size analyzer, which revealed that the mean particle diameter (mD) of S1 was 4.66 μm and that of S2 was 5.21 μm. The formulations were homogenized for 24 hours and had the adjust of their moisture content by adding 7 wt.% of distilled water. Then, the test specimens were shaped under uniaxial pressing in a RIBEIRO-P15T Brasil hydraulic press, applying 15 MPa pressure for 10 seconds and 23 MPa for 20 seconds. The prepared specimens (30 mm x 5 mm x 5 mm) were dried at 110ºC for 24 hours, and some of them had their thermal properties were evaluated by dilatometry, using a NETZSCH DIL 402c dilatometer operating at a maximum temperature of 1300ºC and applying a heating rate of 5ºC/min in an air atmosphere. Test specimens were sintered in a conventional oven furnace (MAITEC INTI with flyever controller FE 50 RP) at temperatures of 1300 and 1400ºC, applying a heating rate of 5ºC/min and dwell times of 2 and 3 hours at the highest temperature.

Crystalline phases identification and quantification were performed using the Internal Standard Method by comparing the strongest peak of the analyzed phases with a standard reference material, corundum (cor). Calculus was performed by the software Shimadzu (Search Match: untitled-XRD: Qualitative Analysis) and JCPDS cards were defined using PCPDFWIN database of the XRD6000 program. The calculation of crystallinity degree was determined using the relation between the integrated area of the amorphous background line and the integrated intensity of the diffraction reflections.

Microstructural characterization was performed by scanning electron microscopy (SEM) using a Shimadzu SSX-550 scanning electron microscope. The dimensions of the mullite needles (length and thickness) were measured, using image analysis software (ImageJ, National Institutes of Health, USA). The following physicomechanical properties were evaluated: linear shrinkage, water absorption, apparent porosity, density, and three point flexural strength. Linear shrinkage values were calculated considering the linear dimensional variation of sintered specimens. Water absorption, apparent porosity and density were determined according to the Archimedes method. The flexural strength of the samples were-analyzed in a Shimadzu Autograph AG-X universal testing machine operating at 0.5 mm/min.

The thermal expansion coefficients (TEC) of the formulations previously sintered at 1300 and 1400ºC were determined. For this, the samples were heated from 25 to 1000ºC, applying a heating rate of 5ºC/min in an air atmosphere, using an equipament BP engineering RB 3000 model dilatometer.

3. Results and Discussion

Figure 1 shows the X-ray diffraction patterns of formulations S1 and S2. A mineralogical analysis of formulations S1 and S2 revealed characteristic peaks of kaolinite (JCPDS: 78-2110), smectite (JCPDS: 29-1499), quartz (JCPDS: 46-1045) and corundum (α-Al_2O_3- JCPDS: 71-1125), which originates from the alumina waste.

Figure 2 shows the thermal expansion curves of the green bodies produced from formulations S1 and S2 and heated to 1300ºC at a heating rate of 5ºC/min in an air atmosphere. The thermal expansion curves of both formulations showed a slight shrinkage that occurred between ~ 100 and ~ 150ºC, which can be attributed to the release of free water, which is consistent with the endothermic peak at ~ 117ºC, as shown

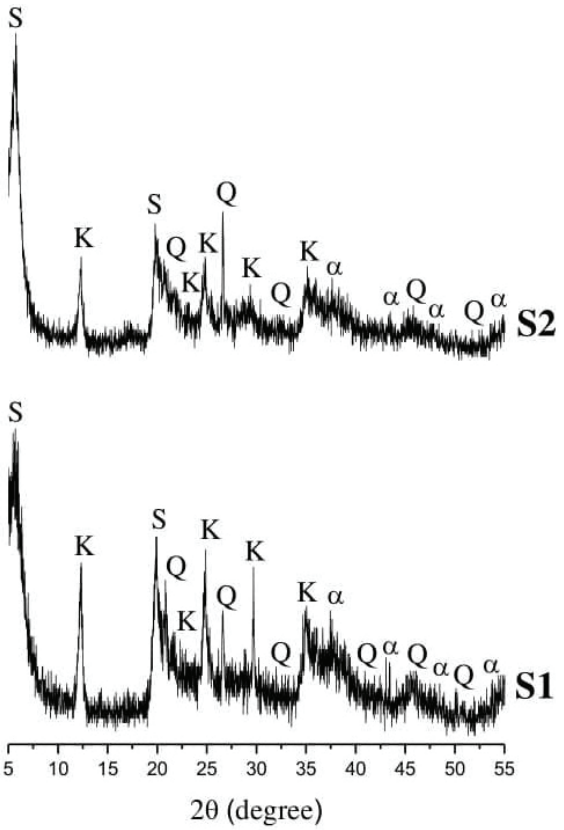

Figure 1. XRD patterns of formulations S1 and S2. *S = smectite; K = kaolinite; Q = quartz and α = α-Al_2O_3 (corundum).*

Table 1. Chemical composition (in %) of formulations S1 and S2.

Formulations	Al_2O_3	SiO_2	F_2O_3	MgO	TiO_2	K_2O	CaO	Other Oxides
S1	56.92	34.21	4.29	2.10	0.65	0.50	0.48	0.85
S2	53.80	38.69	2.87	2.08	0.66	0.29	0.88	0.73

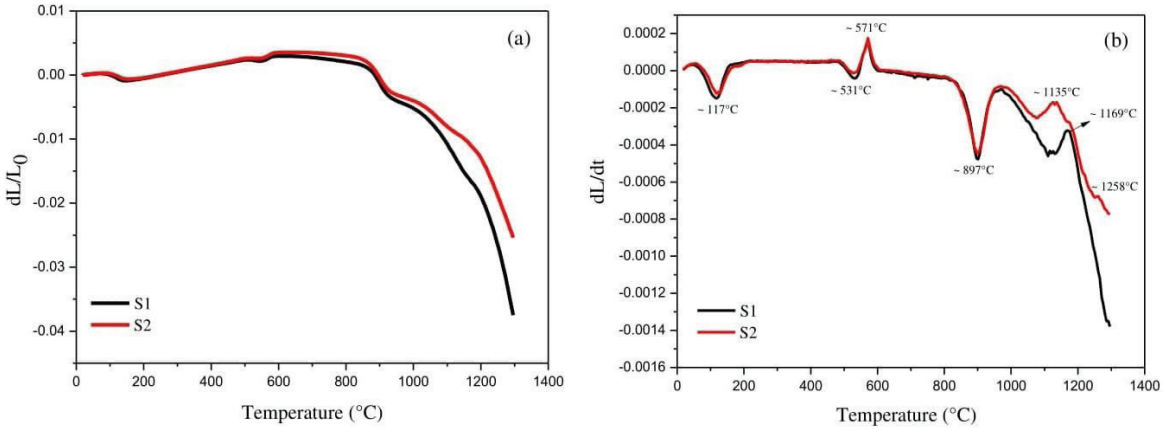

Figure 2. Thermal expansion curves of S1 and S2 green bodies heated to 1300ºC: (a) linear shrinkage curves, and (b) derivative curves.

in Figure 2b. This was followed by a linear expansion in both formulations up to ~ 573ºC, corresponding to the dehydroxylation of the clay minerals and the α→β polymorphic transformation of quartz[26-28]. The region between ~ 851 and ~ 1020ºC was characterized by a structural rearrangement in the clays[26,29] and transformation of the spinel phase into the first mullite crystals, which phase intensified as the temperature increased. Formulations S1 and S2 started to densify at ~ 1182ºC and ~ 1192ºC, respectively. The highest shrinkage occurred in formulation S1, which may be attributed to the larger amount of fluxing oxides in this formulation (Table 1). The derivative curves of both formulations (Figure 2b) showed a change in the crystalline structure of the clays, characterized by an endothermic peak at ~ 531ºC and the transformation of quartz at ~ 571ºC. Exothermic peaks at ~ 1135 and ~ 1258ºC in formulation S2 are indicative of the nucleation and growth of mullite needles, while this phenomenon occurs at ~ 1169ºC in formulation S1. These findings are in agreement with the literature[29].

Figure 3 shows the XRD patterns of the specimens obtained from formulations S1 and S2 sintered at 1300 and 1400ºC, with dwell times at the highest temperature for 2 and 3 hours. The mineralogical analysis of the formulations sintered at 1300ºC revealed characteristic peaks of mullite (JCPDS: 79-1275), quartz (JCPDS: 46-1045) and corundum (α-Al_2O_3 – JCPDS: 10-0173). Increasing the dwell time from 2 to 3 hours contributed to enhance the intensity of the mullite peaks, albeit to the detriment of the corundum and quartz peaks, which declined. Formulation S1 showed the highest peaks of mullite. This may be ascribed to a higher alumina-silica ratio (Al_2O_3/SiO_2), as well as the action of fluxing oxides, which favor the process of liquid phase formation, decreasing the viscosity and accelerating the nucleation of the crystalline phases in this formulation.

Corundum appears as a residual secondary phase due to the excess of alumina in the reaction mixture. According to the literature[30], excessive amounts of alumina can lead to structural rearrangements and the formation of corundum, because mullite is thermodynamically more stable in the alumina/silica system than corundum; hence, the growth of this phase is not expected to cause the dissolution of mullite that has already been formed. In addition to the crystalline phases, note the characteristic band of amorphous phase located at 2Θ ranging from 15 to 30º, which in turn decreases in intensity as the dwell time at the highest temperature increases. The same crystalline phases found in the formulations sintered at 1300ºC were observed when the temperature was increased to 1400ºC, with the exception of quartz. The complete amorphization of quartz, which released silicon ions, and the partial decomposition of corundum, which released aluminum ions, favored greater reactivity, and hence, further intensified the mullite peaks.

Table 2 shows the phase quantification data for formulations S1 and S2 sintered at 1300 and 1400ºC and dwell times of 2 and 3 hours at the highest temperature. As can be seen, the amount of mullite increased along with the increase in temperature and the dwell time at the maximum temperature, to the detriment of corundum and quartz, which levels decreased. In other words, the aluminum and silica ions from the partial decomposition of corundum and quartz reacted, causing a diffusion process that resulted in the formation of larger amounts of mullite at the highest temperatures. It is clear that extending the dwell time from 2 to 3 hours contributed to increase the mullite content, and also resulted in a more than 80% degree of crystallinity. These findings confirm our mineralogical analysis (Figure 3), which indicated a decline in the corundum and quartz peaks, and an increase in the intensity of the mullite peaks. However, both formulations underwent complete amorphization of quartz at 1400ºC.

Formulation S1 showed the highest percentages of mullite, with a content of 92% at 1400ºC for 3 hours. This can be attributed to the following factors: smaller mean particle diameter (mD = 4.66 μm); higher alumina/silica ratio (Al_2O_3/SiO_2 = 1.66) and higher amounts of fluxing oxides (Table 1), which are essential to accelerate the reaction kinetics, thereby favoring the mullitization process. According to the literature[31-33], mullite needles are formed through the recrystallization and dissolution of aluminosilicate in the transient liquid phase. This process can be accelerated by the dissolution-precipitation and the action of the amount of impurity present in the clay composition, e.g., Fe_2O_3, TiO_2, K_2O and Na_2O. In addition, this process occurs in response to the increase of the dissolution rate of alumina (Al_2O_3) in the liquid phase, in which larger proportions of

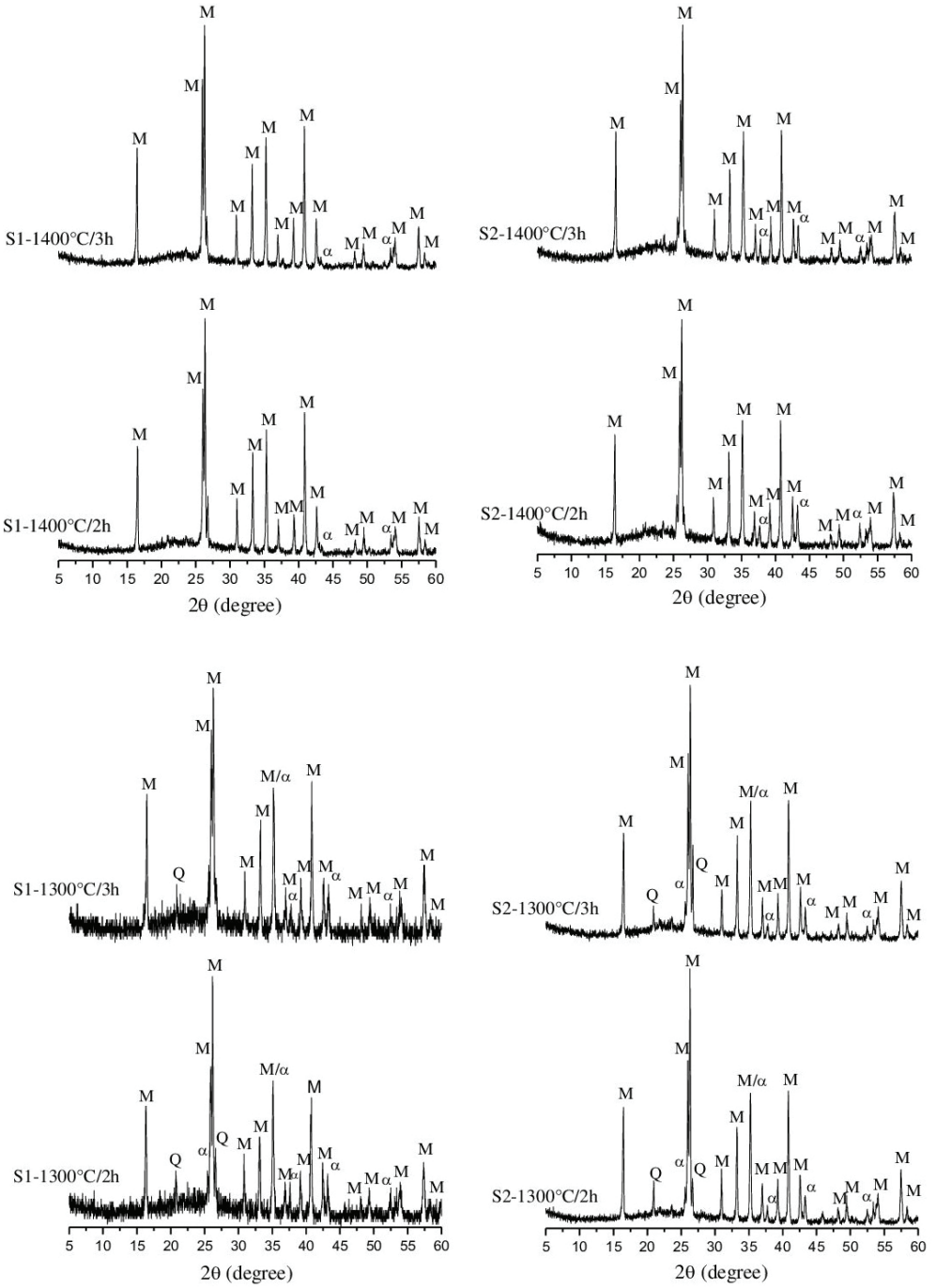

Figure 3. XRD patterns of S1 and S2 test specimens sintered at 1300ºC and 1400º C. *M = mullite*; *Q = quartz*; α = α-Al_2O_3 *(corundum)*.

Table 2. Percent composition of phases in formulations S1 and S2.

Formulations	Mullite	Corundum	Quartz	Crystallinity
S1-1300°C/2h	74.30	10.01	4.02	88.33
S1-1300°C/3h	78.44	6.30	2.01	86.75
S1-1400°C/2h	86.63	1.30	-	87.93
S1-1400°C/3h	92.00	0.55	-	92.55
S2-1300°C/2h	72.83	5.87	8.13	86.83
S2-1300°C/3h	73.00	4.40	5.91	83.31
S2-1400°C/2h	83.20	3.05	-	86.25
S2-1400°C/3h	88.08	1.90	-	89.98

aluminum ions react with the silicon ions from the silica-rich amorphous phase (SiO_2) above 1300ºC, favoring the growth of secondary mullite crystals[3,11,34-36].

Figure 4 shows SEM micrographs of the fracture surface of the specimens obtained from formulations S1 and S2 sintered at 1300ºC with dwell times at 2 and 3 hours the highest temperature. Note the needle-shaped crystals typical of the crystal habit of mullite obtained from clay minerals, which developed into an intricately interwoven arrangement. Small round grains that are also visible can be attributed to the residual secondary phases of corundum and quartz, in addition to the presence of an amorphous phase. These findings are in agreement with the mineralogical analysis (Figure 3).

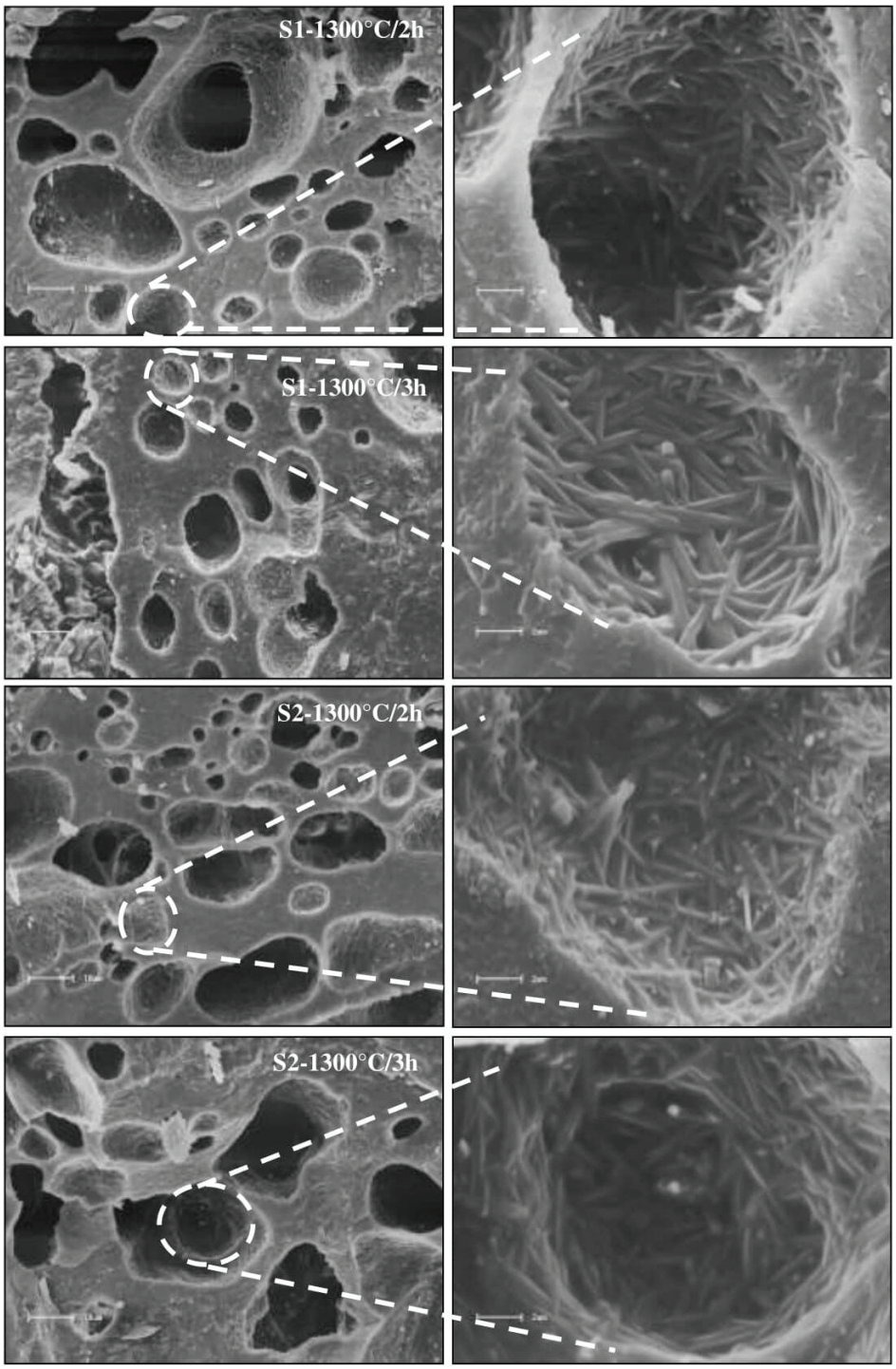

Figure 4. SEM micrographs of the fracture surface of specimens obtained from formulations S1 and S2 sintered at 1300ºC with a dwell time of 2 and 3 hours.

The largest mullite crystals were found in formulation S1-1300ºC/3h. This was attributed to the dwell time at the highest temperature, and to the chemical composition of this formulation (Table 1), which contained the highest levels of fluxing oxides. Several authors[37,38] have stated that to obtain an ideal stoichiometry of mullite from clays is a highly complex procedure, since the aluminosilicate matrix is immersed in a glassy phase. However, it is believed that primary mullite 2:1 derives from the decomposition of clay, while secondary mullite 3:2 is formed by the interaction between clay and the flow of fluxing oxides.

Figure 5 presents SEM micrographs of the fracture surface of specimens produced from formulations S1 and S2, sintered at 1400ºC, with dwell times of 2 and 3 hours at

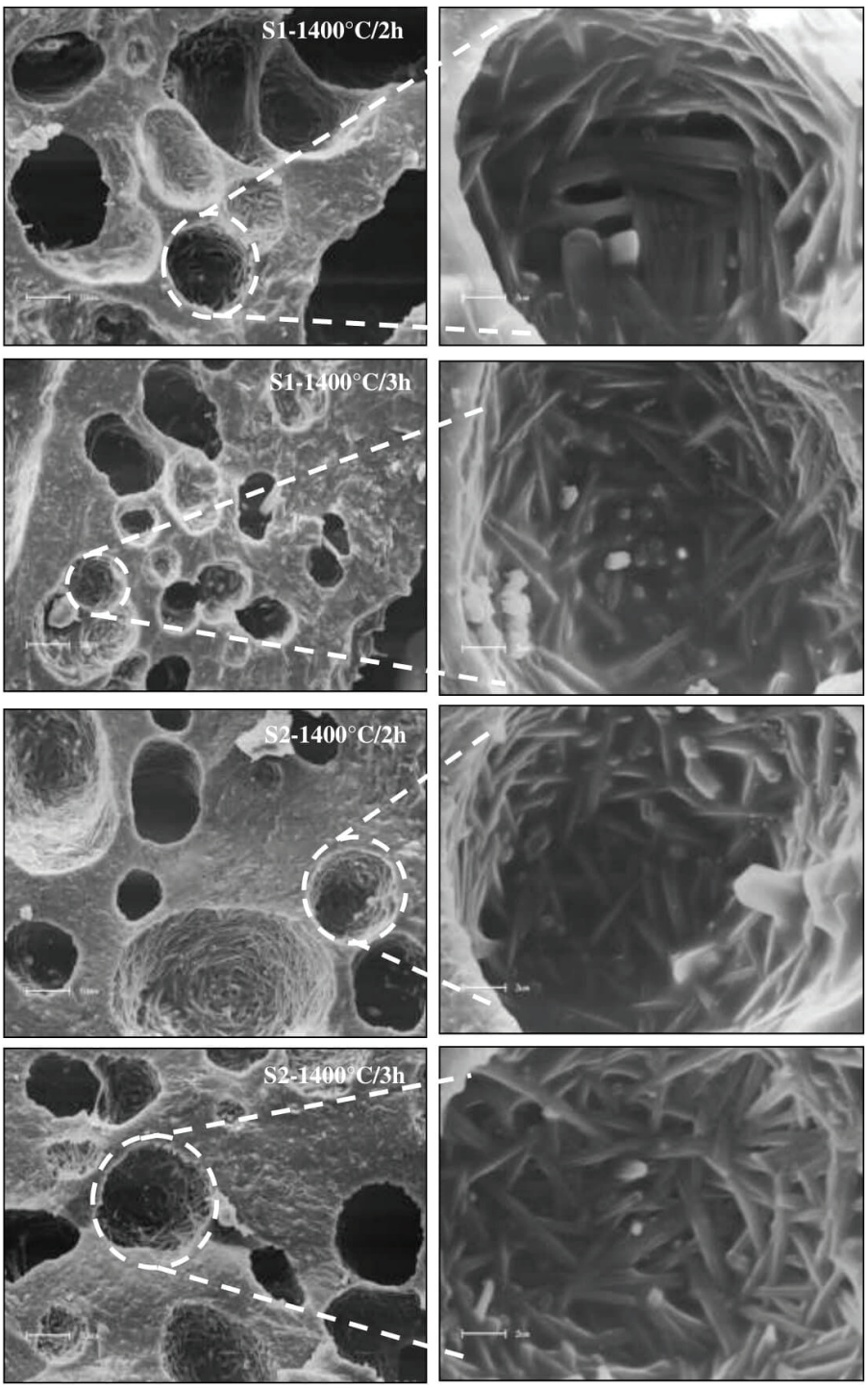

Figure 5. SEM micrographs of the fracture surface of specimens obtained from formulations S1 and S2 sintered at 1400ºC with dwell times of 2 and 3 hours.

the highest temperature. Increasing the sintering time and temperature led to an increase in crystal size, indicating that the silica originating from the complete amorphization of quartz at 1400ºC reacted with the alumina from the corundum, forming more mullite. These crystals are immersed in the glassy phase, which is associated with residual amorphous silica. These findings are consistent with the mineralogical analysis (Figure 3), which revealed a characteristic band of silica-rich amorphous phase located at 2θ varying from 15 to 30º. According to the literature[35], at temperatures between 1200 and 1400ºC, saturation of the silico-aluminous liquid by aluminum ions to reach a condition of equilibrium of the system occurs slowly, due to the low dissolubility of alumina in silica, making the system richer in silicon ions than the equilibrium quantity.

Formulation S1-1400ºC/2h presented the largest mullite crystals, which was attributed to its higher iron oxide (Fe_2O_3) content (Table 1). According to Ganesh and Ferreira[39], precursor materials with silica-rich compositions have long needle-shaped mullite crystals, while alumina-rich compositions tend to have more equiaxed crystals. These morphological characteristics are common in mullite derived from clays, especially when a liquid phase develops during synthesis, due to the presence of fluxing oxides, particularly iron oxide (Fe_2O_3).

Table 3 describes the dimensions (length and thickness) of the mullite needles determined from the SEM images of formulations S1 and S2. As can be seen, the dimensions of the mullite needles increased along with the increase in sintering temperature. The diameters, in general, range from 200 nm (0.2 μm) to 500 nm (0.5 μm). Mullite needles with diameters smaller than 400 nm (0.4 μm) are attributed to the orthorhombic structure, which is considered the most stable one[40].

Table 4 describes the physicomechanical properties of the specimens obtained from formulations S1 and S2 sintered at 1300 and 1400ºC with dwell times of 2 and 3 hours at the highest temperature. As can be seen, in general, the physicomechanical properties improved in response to the increase in temperature and dwell time at the highest temperature. This was probably due to the higher densification of the ceramic bodies, as well as the phases formed during heat treatment, mainly mullite. According to the literature[3,36,41], an increase in the amount of crystalline phases such as cristobalite, mullite and corundum, combined with good densification, considerably improves the mechanical strength of specimens.

By correlating the values presented in Table 4 with the phase quantification data (Table 2) it is clearly seen that the dwell time at maximum temperature contributed to increase the amount of mullite formed, which is the fundamental factor required to increase the flexural strength of ceramic bodies. Also note that there was no significant variation in the linear shrinkage of the ceramic bodies when the dwell time increased from 2 to 3 hours. Needle-shaped mullite crystals usually develop to form an interwoven structure, whose behavior favors an increase in mechanical strength and a reduction in the thermal expansion coefficient[25,31,34,35]. These findings corroborate those reported by Meng and Peng[42], who evaluated the effects of mullite on the flexural strength and fracture toughness of corundum-mullite refractory materials at different temperatures and dwell times at the highest temperature. Formulation S1 presented higher apparent porosity than S2, which can be attributed to the higher iron oxide (Fe_2O_3) content of this formulation (Table 1). According to Chen and Tuan[43], when Fe_2O_3 is converted into Fe_3O_4, it triggers a reaction that releases O_2 at high temperatures, which contributes to lower the density of the ceramic body resulting in the formation of more numerous pores.

Table 3. Dimensions (in μm) of the mullite needles.

Formulations	Length	Diameters	Aspect ratio
S1-1300°C/2h	2.36	0.25	9.44
S1-1300°C/3h	2.88	0.36	7.95
S1-1400°C/2h	5.66	0.46	12.25
S1-1400°C/3h	5.40	0.35	15.43
S2-1300°C/2h	1.94	0.30	6.45
S2-1300°C/3h	2.19	0.27	8.11
S2-1400°C/2h	3.30	0.38	8.68
S2-1400°C/3h	3.81	0.45	8.47

Table 4. Physicomechanical properties of formulations S1 and S2.

Formulations	Water absorption (%)	Apparent porosity (%)	Linear shrinkage (%)	Flexural strength (MPa)	Apparent density (g/cm^3)
S1-1300°C/2h	15.00 ± 0.29	29.00 ± 0.44	6.10 ± 0.05	27.22 ± 1.08	1.75 ± 0.01
S1-1300°C/3h	13.48 ± 0.52	26.30 ± 0.80	6.19 ± 0.09	32.36 ± 1.31	1.76 ± 0.03
S1-1400°C/2h	9.13 ± 0.09	17.70 ± 1.18	8.00 ± 0.05	49.90 ± 2.91	1.81 ± 0.01
S1-1400°C/3h	7.29 ± 0.02	15.90 ± 0.54	8.79 ± 0.01	53.65 ± 2.85	1.85 ± 0.03
S2-1300°C/2h	11.66 ± 0.04	23.00 ± 1.39	5.42 ± 0.02	42.89 ± 1.45	1.79 ± 0.01
S2-1300°C/3h	11.24 ± 0.45	21.82 ± 0.65	5.58 ± 0.07	43.58 ± 1.14	1.78 ± 0.02
S2-1400°C/2h	6.13 ± 0.09	13.10 ± 0.56	7.10 ± 0.05	47.00 ± 1.58	1.82 ± 0.01
S2-1400°C/3h	4.65 ± 0.02	9.34 ± 0.81	7.45 ± 0.08	48.47 ± 1.82	1.85 ± 0.01

Figure 6 shows the thermal expansion curves of the ceramic bodies obtained from formulations S1 and S2 heated to 1000ºC, at a heating rate of 5ºC/min in an air atmosphere. The samples were previously sintered at 1300 and 1400ºC, with dwell times of 2 and 3 hours at the highest temperature. The thermal expansion curves of formulations S1 and S2 showed different behaviors when the samples were reheated. The samples initially sintered at 1300ºC/2h, which underwent α→β phase transition in quartz in the range of 300 to 600ºC, showed a TEC of 6.0 x 10^{-6}°C^{-1} in S1 and of 6.3 x 10^{-6}°C^{-1} in S2. These data are compatible with the phase quantification (Table 2), and the formulation with the highest quartz content was the one with the highest $TEC_{300\text{-}600}$.

An analysis of the specimens previously heated to 1400ºC revealed that those obtained from formulation S2 showed a phase transformation at ~ 950ºC, which, according to Karhu et al.[33], can be attributed to the formation of liquid phase. This transformation was less intense in formulation S1, which be attributed to its higher fluxing oxides content (Table 1) and may have accelerated the phase transformations during the initial heat treatment. This favored the production of larger amounts of crystalline phases, which probably affected the linear and homogeneous behavior observed in the analyzed temperature range.

Table 5 lists the thermal expansion coefficients (TEC) of specimens obtained from formulations S1 and S2, measured by the tangent of the curve at temperature intervals between 25 and 1000ºC. Between 25 and 1000ºC, the TEC values lie within the range of 6.2 to 6.9 x 10^{-6}°C^{-1}, which may be ascribed to the presence of crystalline phases (Table 2), mainly mullite and corundum, which present TEC of ~ 5 to 6 x 10^{-6}°C^{-1} and ~ 7 to 8 x 10^{-6}°C^{-1}, respectively[44-47]. These values are close to those reported by Chen et al.[48], who analyzed the TEC of corundum-mullite composites and found that samples with higher levels of alumina (Al_2O_3) showed higher values of $TEC_{200\text{-}1100}$ of ~ 6 to 7 x $10^{-6}K^{-1}$. Since the specimens obtained in this work contain the same phases, their influence on the thermal properties are probably the same.

The TEC values obtained in this study are also compatible with those obtained by Foo et al.[47], who analyzed compositions containing inorganic wastes to obtain mullite-based ceramics, and suggested that when these precursors are subjected to high temperatures, they generate products that can be employed as refractories. Therefore, mullite-based porous ceramics are promising engineering materials for high temperature

Table 5. Thermal expansion coefficients (TEC) of formulations S1 and S2.

Formulations	$CTE_{25\text{-}1000°C}$ (10^{-6} °C^{-1})
S1-1300/2h	6.2
S1-1300/3h	6.7
S1-1400/2h	6.8
S1-1400/3h	6.8
S2-1300/2h	6.7
S2-1300/3h	6.9
S2-1400/2h	6.8
S2-1400/3h	6.5

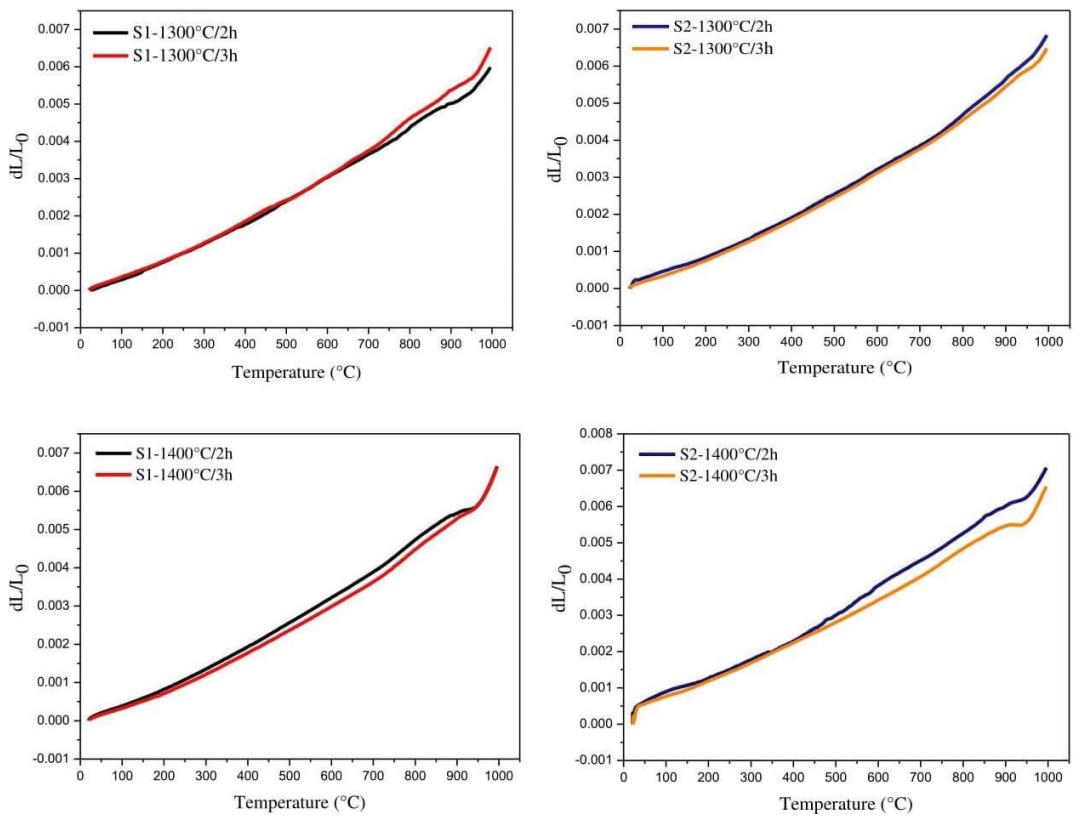

Figure 6. Thermal expansion curves of formulations S1 and S2 previously sintered at 1300 and 1400°C.

applications, since they present a unique combination of factors, such as low thermal expansion coefficient and high thermal shock resistance.

4. Conclusions

Based on the data obtained in this study, the following conclusions can be drawn about the chemical, thermal, mineralogical, microstructural and physicomechanical properties of these refractory ceramics. The predominant crystalline phase was mullite, with percentages above 70%, while corundum and quartz appears as residual phases. The SEM micrographs revealed the formation of needle shaped crystals typical of mullite derived from clay minerals. The samples sintered at 1400ºC showed better physicomechanical properties, particularly the formulation with the highest mullite content (S1-1400ºC/3h), which presented the highest flexural strength. The dilatometric analysis of presintered samples revealed that the presence of mullite and corundum phases enhanced the thermal resistance of the test specimens. Moreover, it should be pointed out that these refractory ceramics not only have high added value but also represent an environmental contribution by using recycled inorganic wastes, thereby significantly reducing the impacts caused by the inappropriate disposal of these wastes or by not subjecting them to proper treatment. These results suggest that the ceramics obtained in this study are suitable for technological applications such as refractory materials or mullite-corundum composites of high mechanical strength.

5. Acknowledgments

The authors gratefully acknowledge the Brazilian research funding agencies CNPq (National Council for Scientific and Technological Development), PIBIC (Institutional Scientific Initiation Scholarship Program)/CNPq – UFCG (Federal University of Campina Grande), and to the National Postdoctoral Program/Capes (PNPD/CAPES/UFCG) for their support of this research.

6. References

1. Stjernberg J, Olivas-Ogaza MA, Anttia ML, Iona JC, Lindblom B. Laboratory scale study of the degradation of mullite/corundum refractories by reaction with alkali-doped deposit materials. Ceram Int. 2013;39:791-800.
2. Hossain SKS, Roy PK. Development of waste derived nano-lakargiite bonded high alumina refractory castable for high temperature applications. Ceram Int. 2019;45:16202-13.
3. Sadik C, El Amrani I-E, Albizane A. Recente advances in sílica-alumina refractory: a review. Journal of Asian Ceramic Societies. 2014;2:83-96.
4. García-Prieto A, Ramos-Lotito M, Gutiérrez-Campos D, Pena P, Baudín C. Influence of microestructural characteristics on fracture toughness of refractory materials. J Eur Ceram Soc. 2015;35:1955-70.
5. Gajo A, Cecinato F. Thermo-mechanical modelling of rock-like materials at very high temperature: application to ceramic refractories. J Eur Ceram Soc. 2016;36:2193-204.
6. Zhang D, Zhou C-H, Lin C-X, Tong DS, Yu WH. Synthesis of clay minerals. Appl Clay Sci. 2010;50:1-11.
7. Roy D, Bagchi B, Das S, Nandy P. Electrical and dielectric properties of sol-gel derived mullite doped with transition metals. Mater Chem Phys. 2013;138:375-83.
8. Sembiring S, Simanjuntak W, Manurung P, Asmi D, Low IM. Synthesis and characterisation of gel-derived mullite precursors from rice husk silica. Ceram Int. 2014;40:7067-72.
9. Hammel EC, Ighodaro LR, Okoli OI. Processing and properties of advanced porous ceramics: an application-based review. Ceram Int. 2014;40:15351-70.
10. Schneider H, Fischer RX, Schreuer J. Mullite: crystal structure and related properties. J Am Ceram Soc. 2015;98:2948-67.
11. Kool A, Thakur P, Bagchi B, Hoque NA, Das S. Mechanical, dielectric and photoluminescence properties of alumina-mullite composite derived from natural Ganges clay. Appl Clay Sci. 2015;114:349-58.
12. Obada DO, Dodoo-Arhin D, Dauda M, Anafi FO, Ahmed AS, Ajayi OA. Potentials of fabricating porous ceramic bodies from kaolin for catalytic substrate applications. Appl Clay Sci. 2016;132-133:194-204.
13. Alves HPA, Junior RA, Campos FA, Dutra RPS, Grilo JPF, Loureiro FJA, et al. Structural study of mullite based ceramics derived from a mica-rich kaolin waste. Ceram Int. 2017;43:3919-22.
14. Bhardwaj A, Hossain SKS, Majhi MR. Preparation and characterization of clay bonded high strength silica refractory by utilizing agriculture waste. Bol Soc Esp Ceram Vidr. 2017;56:256-62.
15. Sobrosa FZ, Stochero NP, Marangon E, Tier MD. Development of refractory ceramics from residual silica derived from rice husk ash. Ceram Int. 2017;43:7142-6.
16. Almeida EP, Brito IP, Ferreira HC, Lira HL, Santana LNL, Neves GA. Cordierite obtained from compositions containing kaolin waste, talc and magnesium oxide. Ceram Int. 2018;44:1719-25.
17. Kalil NM, Algamal Y, Saleem QM. Exploitation of petroleum waste sludge with local bauxite raw material for producing high-quality refractory ceramics. Ceram Int. 2018;44:18516-27.
18. Ramezani A, Emami SM, Nemat S. Effect of waste serpentine on the properties of basic insulating refractories. Ceram Int. 2018;44:9269-75.
19. Hadi EM, Hussein SI. A sustainable method for Porous refractory ceramic Manufacturing from kaolin by adding of burned and raw wheat straw. Energy Procedia. 2019;157:241-53.
20. Hossain SKS, Roy PK. Fabrication of sustainable insulation refractory: utilization of different wastes. Bol Soc Esp Ceram Vidr. 2019;58:115-25.
21. Brito IP, Almeida EP, Neves GA, Lira HL, Menezes RR, Silva VJ, et al. Development of cordierite/mullite composites using industrial wastes. Internatioanl Jouranl of Applied Ceramic Technology. 2020;00:1-9.
22. Haddar AE, Manni A, Azdimousa A, Hassari I-EA, Bellil A, Sadik C, et al. Elaboration of a high mechanical performance refractory from halloysite and recycled alumina. Bol Soc Esp Ceram Vidr. 2020;59:95-104.
23. Hossain SKS, Roy PK. Waste rice husk ash derived sol: apotential binder in high alumina refractory castables as a replacement of hydraulic binder. J Alloys Compd. 2020;817:152806.
24. Qi J, Yan W, Chen Z, Schafföner S, Zhou W, Li G, et al. Preparation and characterization of microporous mullite-corundum refractory aggregates with high strength and closed porosity. Ceram Int. 2020;46:8274-80.
25. Silva VJ, Silva MJ, Gonçalves WP, Menezes RR, Neves GA, Lira HL, et al. Porous mullite blocks with compositions containing kaolin and alumina waste. Ceram Int. 2016;42:15471-8.

26. Kam S, Zerbo L, Bathiebo J, Soro J, Naba S, Wenmenga U, et al. Permeability to water of sintered clay ceramics. Appl Clay Sci. 2009;46:351-7.
27. M'barek Jemai MB, Karoui-Yaakoub N, Sdiri A, Salah IB, Azouzi R, Duplay J. Late cretaceous and Palaeoceme clays of the Northen Tunisia: potentiel use for manufacturing clay products. Arab J Geosci. 2015;8:11135-48.
28. Sousa LL, Salomão R, Arantes VL. Development and characterization of porous moldable refractory structures of the alumina-mullite-quartz system. Ceram Int. 2017;43:1362-70.
29. Zouaoui H, Lecomete-Nana GL, Krichen M, Bouaziz J. Structure, microstructure and mechanical features of ceramic products of clay and non-plastic clay mixtures from Tunisia. Appl Clay Sci. 2017;135:112-8.
30. Ribeiro MJ, Tulyagavov DU, Ferreira JM, Labrincha JA. High temperature mullite dissolution in ceramic bodies derived from Al-rich sludge. J Eur Ceram Soc. 2005;25:703-10.
31. Hou Z, Cui B, Liu L, Liu Q. Effect of the different additives on the fabrication of porous kaolin based mullite ceramics. Ceram Int. 2016;42:17254-8.
32. Zhu Z, Wei Z, Shen J, Zhu L, Xu L, Zhang Y, et al. Fabrication and catalytic growth mechanism of mullite ceramic whiskers using molybdenum oxide as catalyst. Ceram Int. 2017;43:2871-5.
33. Karhu M, Lagerbom J, Solismaa S, Honkanen M, Ismailov A, Räisänen M-L, et al. Mining tailings as raw materials for reaction-sintered aluminosilicate ceramics: effect of mineralogical composition on microstructure and properties. Ceram Int. 2019;45:4840-8.
34. Guo A, Liu J, Xu R, Xu H, Wang C. Preparation of mullite from desilication-flyash. Fuel. 2010;89:3630-6.
35. Xu L, Xi X, Shui A, Zhu W. Preparation of mullite whisker skeleton porous ceramic. Ceram Int. 2015;41:11576-9.
36. Xu X, Li J, Wu J, Tang Z, Chen L, Li Y, et al. Preparation and thermal shock resistance of corundum-mullite composite ceramics from andalusite. Ceram Int. 2017;43:1762-7.
37. Schneider H, Okada K, Pask JA. Mullite and mullite ceramics. Chichester, UK: John Wiley and Sons; 1994.
38. Lee WE, Souza GP, McConville CJ, Tarvornpanich T, Iqbal Y. Mullite formation in clays and clay-derived vitreous ceramics. J Eur Ceram Soc. 2008;28:465-71.
39. Ganesh I, Ferreira JMF. Influence of raw material type and of the overall chemical composition on phase formation and sintered microstructure of mullite aggregates. Ceram Int. 2009;35:2007-15.
40. Park YM, Yang TY, Yoon SY, Stevens R, Park HC. Mullite whiskers derived from coal fly ash. Mater Sci Eng A. 2007;454-455:518-22.
41. Shimizu T, Matsuura K, Furue H, Matsuzak K. Thermal conductivity of high porosity alumina refractory bricks made by a slurry gelation and foaming method. J Eur Ceram Soc. 2013;33:3429-35.
42. Meng B, Peng J. Effects of in situ synthesized mullite whiskers on flexural strength and fracture toughness of corundum-mullite refractory materials. Ceram Int. 2013;39:1525-31.
43. Chen CY, Tuan WH. The processing of kaolin powder compact. Ceram Int. 2001;27:795-800.
44. Meléndez-Martínez J, Jiménez-Melendo M, Domínguez-Rodríguez A, Wötting G. High temperature mechanical behavior of aluminium titanate-mullite composites. J Eur Ceram Soc. 2001;21:63-70.
45. Aksel C. The effect of mullite on the mechanical properties and thermal shock behavior of alumina–mullite refractory materials. Ceram Int. 2003;29:183-8.
46. Nakata M, Suganuma K. Effect of internal structure on thermal properties of alumina/aluminum composites fabricated by gelate-freezing and partial-sintering process, respectively. Mater Trans. 2005;46:130-5.
47. Foo CT, Salleha MAM, Ying KK, Matori KA. Mineralogy and thermal expansion study of mullite-based ceramics synthesized from coal fly ash and aluminum dross industrial wastes. Ceram Int. 2019;45:7488-94.
48. Chen M, Gao S, Xu L, Wang N. High temperature mechanical and corrosion resistance of Fe-containing MgO-C refractory in oxidizing atmosphere. Ceram Int. 2019;45:21023-2108.